$\frac{l}{2}$ mil

NASA TECHNICAL NOTE

NASA TN D-7394

D-7394

NASA TN

WIND-TUNNEL ROLL-DAMPING MEASUREMENTS OF A WINGED SPACE SHUTTLE CONFIGURATION IN LAUNCH ATTITUDE

by Robert W. Hess and Edwin E. Davenport

Langley Research Center
Hampton, Va. 23665

1. Report No. NASA TN D-7394	2. Government Accession No.	3. Recipient's Catalog No.
4. Title and Subtitle WIND-TUNNEL ROLL-DAMPING MEASUREMENTS OF A WINGED SPACE SHUTTLE CONFIGURATION IN LAUNCH ATTITUDE		5. Report Date December 1973
		6. Performing Organization Code
7. Author(s) Robert W. Hess and Edwin E. Davenport		8. Performing Organization Report No. L-8991
9. Performing Organization Name and Address NASA Langley Research Center Hampton, Va. 23665		10. Work Unit No. 502-32-02-03
		11. Contract or Grant No.
12. Sponsoring Agency Name and Address National Aeronautics and Space Administration Washington, D.C. 20546		13. Type of Report and Period Covered Technical Note
		14. Sponsoring Agency Code

15. Supplementary Notes

16. Abstract

    Ground-wind load studies were conducted on three model configurations to assess the importance of aeroelastic instabilities of erected space shuttle vehicles. Roll damping was measured on a fuselage-alone model, which had a "D" cross section, and a fuselage and tail surfaces in combination with either a clipped-delta wing or a low-sweep tapered wing as the primary lifting surface. The largest negative roll-damping coefficients were measured with the fuselage-alone configuration and were a function of wind azimuth. At the wind azimuths at which the wing-fuselage configuration was unstable, the negative roll-damping coefficients were a function of reduced frequency.

17. Key Words (Suggested by Author(s)) Ground-wind loads Galloping instability Space shuttle		18. Distribution Statement Unclassified — Unlimited		
19. Security Classif. (of this report) Unclassified	20. Security Classif. (of this page) Unclassified		21. No. of Pages 23	22. Price* Domestic, $2.75 Foreign, $5.25

WIND-TUNNEL ROLL-DAMPING MEASUREMENTS OF A WINGED SPACE
SHUTTLE CONFIGURATION IN LAUNCH ATTITUDE

By Robert W. Hess and Edwin E. Davenport
Langley Research Center

SUMMARY

Ground-wind load studies were conducted on three model configurations to assess
the importance of aeroelastic instabilities of erected space shuttle vehicles. Roll damping
was measured on a fuselage-alone model, which had a "D" cross section, and a fuselage
and tail surfaces in combination with either a clipped-delta wing or a low-sweep tapered
wing as the primary lifting surface. The largest negative roll-damping coefficients were
measured with the fuselage-alone configuration and were a function of wind azimuth. At
the wind azimuths at which the wing-fuselage configuration was unstable, the negative roll-
damping coefficients were a function of reduced frequency.

INTRODUCTION

Instabilities which result from flow separation on noncircular cross sections and on
lifting surfaces (characterized by the names "galloping" and "stop-sign flutter" in refs. 1,
2, and 3) were considered in early designs of the space shuttle booster configuration. In
order to investigate the severity of such aeroelastic instabilities on space shuttle config-
urations, a model was constructed with interchangeable lifting surfaces so that three basic
configurations could be studied. The three model configurations were the fuselage alone,
which had a "D" cross section, and the fuselage and tail surfaces with either a tapered
straight wing or a delta wing as a primary lifting surface.

Damping-in-roll derivatives were measured on the three models by means of forced-
oscillation techniques over a range of frequency, dynamic pressure, and wind azimuth
angle.

SYMBOLS

b   fuselage width or wing span

C_{l_p} damping-in-roll parameter (about body axis), see equation (1)

1

f   frequency

k   reduced-frequency parameter, $\dfrac{\omega b}{2V}$

m   mass

q   dynamic pressure, $\dfrac{1}{2}\rho V^2$

R   Reynolds number based on a length of 0.305 m (1 ft)

r   radius

r_Φ radius of gyration about roll axis

S   total model projected planform area

$T_j = T_X \sin \lambda$

T_X average torque required to drive model

V   velocity

ζ ratio of damping to critical value

λ phase angle between torque and displacement

ρ air density

Φ amplitude of angular displacement oscillations about model longitudinal axis

ϕ wind azimuth angle measured between wind vector and model plane of
                symmetry ($\phi = 0^\circ$ when underside of fuselage faces upstream)

ω circular frequency, $2\pi f$

Dots indicate derivatives with respect to time.

MODELS AND EQUIPMENT

Wind Tunnel

The study was made in the Langley high-speed 7- by 10-foot tunnel, which is a continuous-flow, subsonic, atmospheric wind tunnel capable of Mach numbers to 0.9. The test section is 2.007 meters high and 2.921 meters wide with a usable test-section length of 3.098 meters.

Models

Three model configurations were tested: fuselage alone, fuselage with tail surfaces and a tapered wing, and fuselage with tail surfaces and a 50° clipped-delta wing. For convenience, the three models are referred to as configuration I, II, and III, respectively. Geometric details of the three configurations are given in figure 1. The models were constructed of fiber glass and plastic foam with appropriate aluminum inserts used to transmit loads from the lifting surfaces to the model fuselage. They were not elastically scaled. Model properties such as mass, inertia about the roll axis, and still-air natural frequencies are given in table I.

Oscillating Sting Balance

An oscillating sting balance system, adapted from the roll apparatus described in reference 4, was used to determine the damping-in-roll derivatives by means of a forced-oscillation technique. The models were mounted on the oscillating sting balance which was attached to the sidewall of the tunnel with the fuselage longitudinal axis normal to the tunnel sidewall. (See fig. 2.) This system could be rotated to vary the wind azimuth angle from $\phi = -10^\circ$ to $\phi = 190^\circ$, where ϕ is 0° when the bottom of the fuselage is facing upstream. A 1.49-kW, variable-speed motor oscillated the sting and the model by means of an offset crank to give a sinusoidal motion in roll with an amplitude of $\Phi = \pm 2.50^\circ$. Figure 3 shows some details of the oscillating sting mechanism adapted to the tunnel side-wall. The stationary torsion spring internal to the sting is connected to the oscillating outer shaft by a flexure diaphragm. The torsion spring provides a restoring torque which together with the aerodynamic spring component balances out the model internal forces. The strain-gage balance, which is forward of all the bearings and other friction-producing devices, senses only the aerodynamic forces. A system of resolvers and filters is used to separate the torque into in-phase and out-of-phase components with roll displacement. The component of torque which is 90° out of phase with the sting-model displacement is due to aerodynamic damping.

ROLL-DAMPING MEASUREMENTS

For each configuration, a preliminary wind-azimuth sweep was made from $\phi = 0^\circ$ to $\phi = 180^\circ$ in 10° increments to identify regions of negative aerodynamic damping. The dynamic pressure was held constant at 247 N/m^2. At each azimuth angle the roll frequency was varied over a range from 2 Hz to 8 Hz, which included the resonant frequency for each configuration.

Over the range of azimuth angle where the aerodynamic damping was found to be negative, measurements of roll-damping coefficient were made in more detail. The azimuth-angle increments were reduced to 5° and the measurements were made over a range of dynamic pressure up to a maximum of 1220 N/m^2. As in the preliminary sweep the roll frequency was varied over a range from 2 Hz to 8 Hz at each increment of azimuth.

The roll-damping coefficient was determined by methods developed in reference 5. The roll-damping coefficient with respect to the body axis was computed as

$$-C_{l_p} = \frac{2V}{qSb^2}\left[\left(\frac{T_j}{\omega\Phi}\right)_{\text{wind on}} - \left(\frac{T_j}{\omega\Phi}\right)_{\text{wind off}}\right] \tag{1}$$

The wind-off or tare value of $T_j/\omega\Phi$ is obtained at the resonant frequency of the system, that is, when the inertia forces exactly counteract the spring forces. Experience has shown that damping measurements at off-resonant frequencies may be used to establish stability conditions.

RESULTS AND DISCUSSION

Roll-Damping Measurements

The results of a preliminary survey in which wind azimuth angle was varied to determine areas of instability are shown in figure 4 (open symbols) for each of the three configurations. This survey was made at a constant value of reduced frequency and Reynolds number. The variation of the roll-damping coefficient C_{l_p} is plotted as a function of the wind azimuth angle ϕ. An examination of the results in figure 4 indicates that the addition of lifting surfaces to the fuselage has changed the azimuth-angle regions in which negative roll damping occurs. The changes in roll damping with increasing root chord are indicated in figure 4, where configurations I and II have negative roll coefficients at wind azimuth angles from 0° to 20° whereas configuration III is stable in this region. (The root chords of the lifting surfaces are 22.4 percent of the fuselage length for configuration II and 54 percent of the fuselage length for configuration III.) Moreover,

4

the largest value of the negative roll-damping coefficient was measured on configuration I. The data for configuration I, figure 4(a), are given by two sets of symbols. The open symbols are for a wind-azimuth sweep with $k = 0.1695$ at a constant Reynolds number, based on a length of 0.305 m (1 ft), of 0.426×10^6. The solid symbols, which represent slightly different values of k and Reynolds number, indicate that large negative roll damping occurs near $\phi = 17^o$. As is shown in reference 6, the static side force on a noncircular cylinder is sensitive to cross-section shape and azimuth angle. This sensitivity is illustrated by the behavior of the configuration of the present study, which shows large changes in roll damping over a narrow range of azimuth angle.

The regions in which the wind-azimuth sweeps indicated that the roll damping was small or negative were examined in detail by varying reduced frequency in small increments. The data are plotted in figure 5 for discrete azimuth angles in the regions of interest. A boundary drawn as a dashed line is faired through the minimum values of the roll-damping coefficient. A difference in the nature of the instability between the fuselage alone (configuration I) and the wing-fuselage configurations (configurations II and III) is shown in figure 5. In an azimuth-angle region where the aerodynamic damping in roll $-C_{l_p}$ is negative, the degree to which it is negative is a more sensitive function of azimuth angle, and to a lesser degree of reduced frequency, for configuration I than for configurations II and III. Configurations II and III are more sensitive than configuration I to variations in k.

Instability Mechanisms

Negative aerodynamic damping in roll for the fuselage alone can be generated by two mechanisms that are associated with unsteady lift forces acting normal to the airstream, provided that the location of the center of pressure is such that the resultant vector of the unsteady lift forces does not pass through the balance center of the body. These two mechanisms are vortex-shedding and "galloping" instability.

Vortex-shedding instability is associated with unsteady lift forces produced by vortices alternately shed from each side of a bluff body. The conditions for which vortices may be expected to shed periodically from a cylinder of diameter D with a frequency f are a function of Strouhal number fD/V and Reynolds number. In this study the Strouhal number varied from 0.015 to 0.086 for configuration I and from 0.0097 to 0.086 for configurations II and III. These values are well below values (0.21) at which unsteady lift due to vortex shedding may be expected (ref. 7) for the range of Reynolds number of the present study. The negative aerodynamic damping in roll measured with configuration I would therefore appear to be the result of galloping instability (refs. 1 to 3).

Galloping instability is basically a static aerodynamic phenomenon that is associated with noncircular cross sections (ref. 3) and is dependent upon Reynolds number. The

5

instability results from movement of the fuselage normal to the airstream, which results in an effective angle-of-attack change. In the tests under discussion, the relative wind angle was varied by oscillating the model in roll rather than translation due to bending. If the angle of attack is such that the resulting lift forces are in the direction of fuselage movement (positive), the system is unstable. This was shown to be the case for a cylinder of rectangular cross section with rounded corners at azimuth angles of 5° and 10° in reference 6. Positive static side forces reported in reference 6 were for Reynolds numbers up to about 1.1×10^6, which encompasses the Reynolds number range of the present test.

It is to be expected that the addition of lifting surfaces to configuration I would alter the results because a new source of instability has been introduced. A possible source of this instability, characterized by the name "stop-sign flutter" in reference 1, is flow separation from the lifting surfaces. It is a phenomenon similar to stall flutter in that it involves negative aerodynamic damping in the torsional mode, in this case about the vehicle longitudinal axis rather than a wing axis.

Although it is not possible, with the available data, to ascribe the source of negative damping at a given azimuth angle for configurations II and III, some observations can be made. At the azimuth angles where galloping instability was most severe for configuration I ($\phi = 0°$ to $\phi = 20°$), the extent of negative damping decreases with the addition of lifting surfaces, so that configuration III (with a ratio of root chord to fuselage length of 54 percent) has positive damping in roll. At azimuth angles where negative damping was not observed with configuration I, instabilities were observed for configurations II and III (fig. 4). Since these instabilities are not at azimuth angles associated with galloping, stop-sign flutter is a primary candidate as the responsible mechanism. However, the flow is complex and other nonpotential flow sources are a possibility.

Stability Boundaries

As in reference 1, an idealized mass representation of the model may be used to relate the pertinent structural and aerodynamic parameters of this investigation. The differential equation of motion for model rotation about the roll axis may be written

$$mr_\Phi^2\left(\ddot{\Phi} + 2\omega\zeta\dot{\Phi} + \omega^2\Phi\right) = -M_{aero} \tag{2}$$

The terms on the left side of equation (2) are associated with the inertia, damping, and stiffness properties of the structure. The expression on the right side M_{aero} represents the aerodynamic moment acting on the body and consists of aerodynamic terms that are the counterparts of the structural terms on the left side of the equation (including an aerodynamic-damping term $\rho SbC_{lp}\frac{b}{2V}$). These terms relate to the interaction of the

6

body motion and the local unsteady flow field. In order to assess the stability of the con-
figuration, only the damping terms of the equation need be considered for this single-
degree-of-freedom representation. Neutral stability occurs when the total damping term
vanishes, that is,

$$2\omega\zeta + \frac{qSb}{mr_\Phi^2}\left(-C_{l_p}\right)\frac{b}{2V} = 0 \tag{3}$$

This relation may be reorganized to form a nondimensional expression relating the roll-
damping coefficient $-C_{l_p}$ and the reciprocal of the Strouhal number V/fb to a damping-
inertia parameter $\zeta\left(\frac{m}{\rho Sb}\right)\left(\frac{r_\Phi}{b}\right)^2$:

or

$$\left.\begin{array}{l}\zeta\left(\dfrac{m}{\rho Sb}\right)\left(\dfrac{r_\Phi}{b}\right)^2 = \dfrac{C_{l_p}}{16\pi}\left(\dfrac{V}{fb}\right)\\[4mm]\zeta\left(\dfrac{m}{\rho Sb}\right)\left(\dfrac{r_\Phi}{b}\right)^2 = \dfrac{C_{l_p}}{8}\left(\dfrac{1}{k}\right)\end{array}\right\} \tag{4}$$

In this parameter, ζ is the critical damping ratio of the structure; $m/\rho Sb$ is the
mass-ratio parameter involving the total planform area S and fuselage width or wing
span b; and r_Φ is the radius of gyration of the vehicle about the roll axis.

Values of the reciprocal of the Strouhal number for negative values of $-C_{l_p}$ were
determined for a particular configuration and test condition from the minimum damping
boundaries of figure 5. These values of $-C_{l_p}$ and V/fb were substituted into equa-
tion (4) to obtain the damping-inertia parameter for neutral stability of the three config-
urations shown in figure 6. The region of instability for each configuration is above the
curve. The wing-fuselage configurations have similar boundaries, although the delta-
wing configuration has a slightly lower boundary over the range of variables tested. The
fuselage-alone configuration is significantly different from the wing-fuselage configura-
tions in that the instability region extends over a greater range of the damping-inertia
parameter. For reduced velocities above a value of approximately 8, the lifting surfaces
evidently reduced the negative damping. As was discussed in the previous section, this
may be due to the fact that the nature of the instability was altered with the addition of
the lifting surfaces. The shaded area in figure 6 indicates the stability region for an
early design of the space shuttle booster. As is shown in the figure, the booster design
falls well below the region where the instabilities were observed in this study.

CONCLUDING REMARKS

Instabilities which result from flow separation on noncircular cross sections and on lifting surfaces at high angles of attack, such as space shuttle booster configurations in a launch attitude exposed to ground winds, have been studied by measuring the roll-damping coefficients of wind-tunnel models. A model with interchangeable lifting surfaces was used to study three basic configurations: a fuselage alone having a "D" cross section, and this same fuselage with tail surfaces and with either a low-sweep tapered wing or a clipped-delta wing as the primary lifting surface.

Negative aerodynamic damping in roll was measured on all three configurations. The largest value of negative aerodynamic damping coefficient was measured on the fuselage alone. The addition of lifting surfaces to the fuselage resulted in lower values of negative aerodynamic damping which occurred over a comparatively wider range of wind azimuth angle and reduced frequency. "Galloping" instability was identified as the source of the negative roll damping measured with the fuselage-alone model since the Strouhal number was too low over the range of Reynolds number of the study for vortex shedding to be a consideration. "Stop-sign flutter" was the likely mechanism of the wing-fuselage instability, but because of the complex flow for this configuration, other sources of instability are a possibility.

Langley Research Center,
    National Aeronautics and Space Administration,
        Hampton, Va., October 12, 1973.

REFERENCES

1. Reed, Wilmer H., III: Wind Effects on Space Shuttle Vehicles Erected on Launch Pad. Proceedings of the Third International Conference on Wind Effects on Buildings and Structures, Japanese Organizing Comm., eds., Saiko Co., Ltd. (Tokyo), 1971. pp. 1127-1140.

2. Richardson, A. S., Jr.; Martuccelli, J. R.; and Price, W. S.: Research Study on Galloping of Electric Power Transmission Lines – Pt. I. Wind Effects on Buildings and Structures, Vol. II, Her Majesty's Stationery Office, 1965, pp. 612-686.

3. Den Hartog, J. P.: Mechanical Vibrations. Fourth ed., McGraw-Hill Book Co, Inc., 1956.

4. Boyden, Richmond P.: Theoretical and Experimental Studies of the Effects of Leading-Edge Vortex Flow on the Roll Damping of Slender Wings. AIAA Paper No. 70-540, May 1970.

5. Braslow, Albert L.; Wiley, Harleth G.; and Lee, Cullen Q.: A Rigidly Forced Oscillation System for Measuring Dynamic-Stability Parameters in Transonic and Supersonic Wind Tunnels. NASA TN D-1231, 1962.

6. Polhamus, Edward C.: Effect of Flow Incidence and Reynolds Number on Low-Speed Aerodynamic Characteristics of Several Noncircular Cylinders With Applications to Directional Stability and Spinning. NASA TR R-29, 1959. (Supersedes NACA TN 4176.)

7. Jones, George W., Jr.; Cincotta, Joseph J.; and Walker, Robert W.: Aerodynamic Forces on a Stationary and Oscillating Circular Cylinder at High Reynolds Numbers. NASA TR R-300, 1969.

TABLE I.- MODEL PARAMETERS

Configuration	I	II	III
Wing aspect ratio	-----	7.59	2.56
Wing taper ratio	-----	0.417	0.152
Wing dihedral, deg	-----	7	1.0
Planform reference area, S, m^2	0.324	0.527	0.784
Reference span, b, m	0.216	1.207	1.207
Natural frequency for system in roll, f, Hz	7.25	4.25	3.51
Mass, kg	0.1379	0.1845	0.1995
Mass moment of inertia about roll axis, kg-m^2	0.0537	0.1554	0.2268
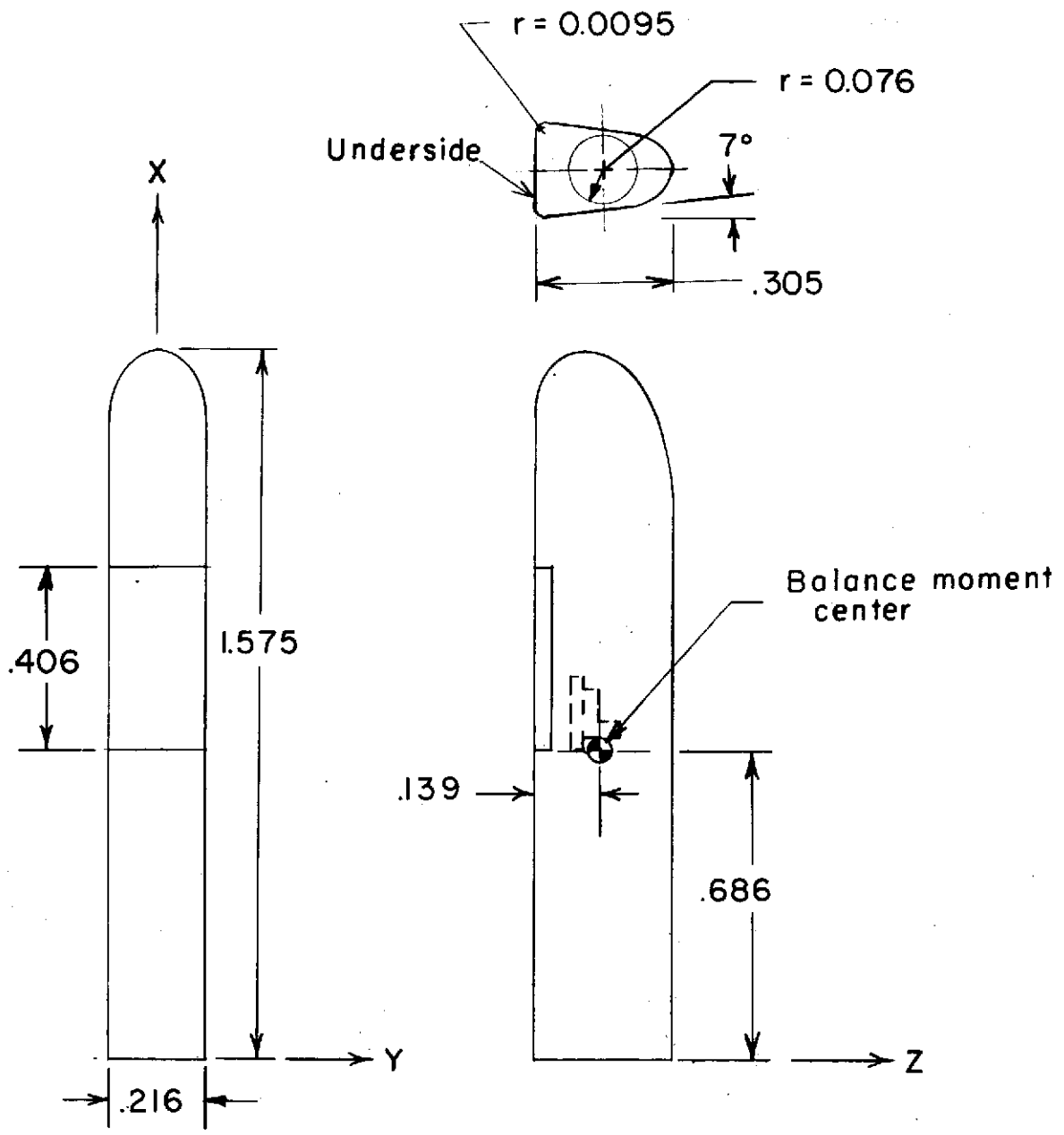
(a) Configuration I.

Figure 1.- Model dimensions.   Linear dimensions are in meters.
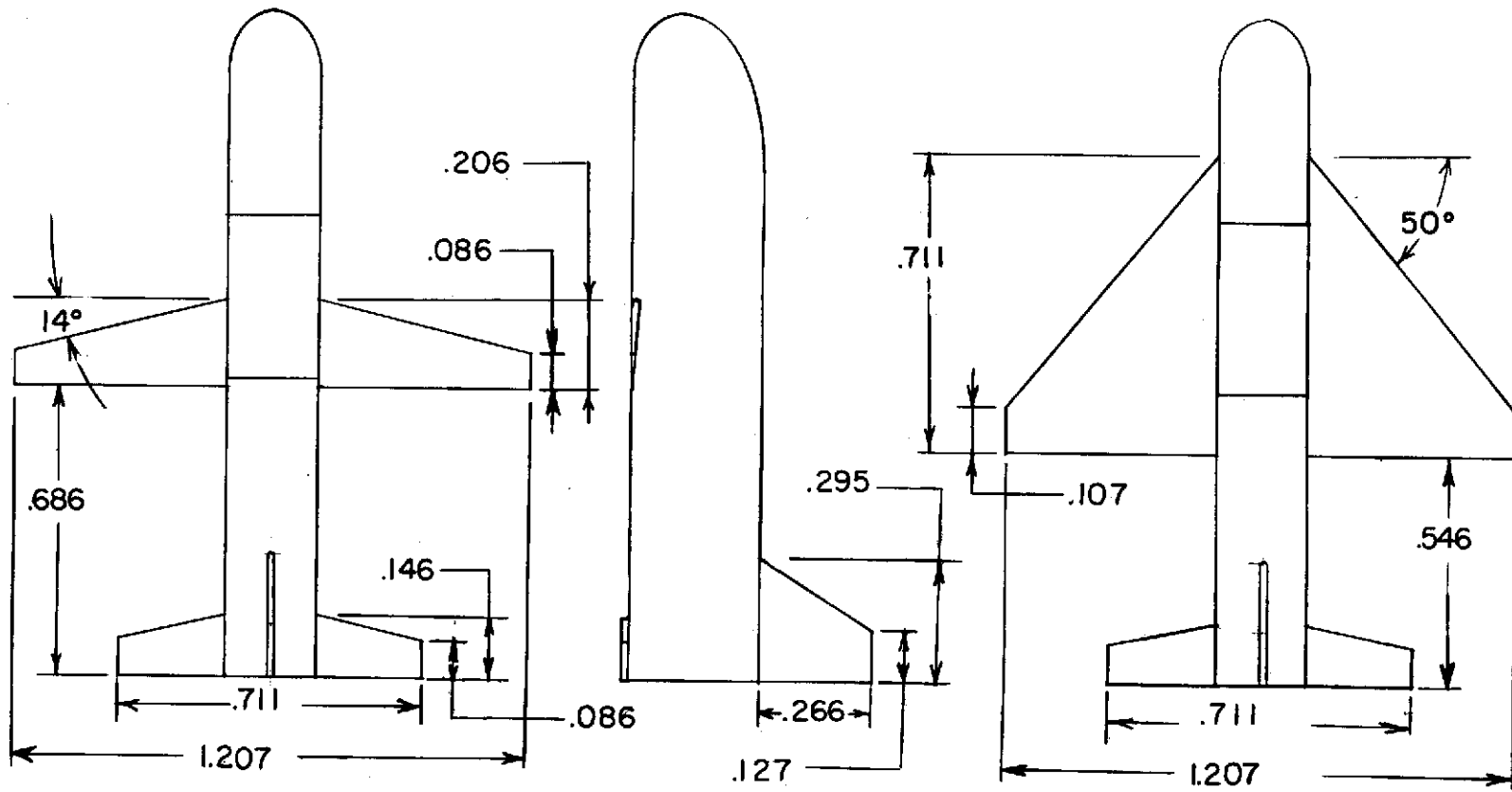
(b) Configuration II.

(c) Configuration III.

Figure 1.- Concluded.
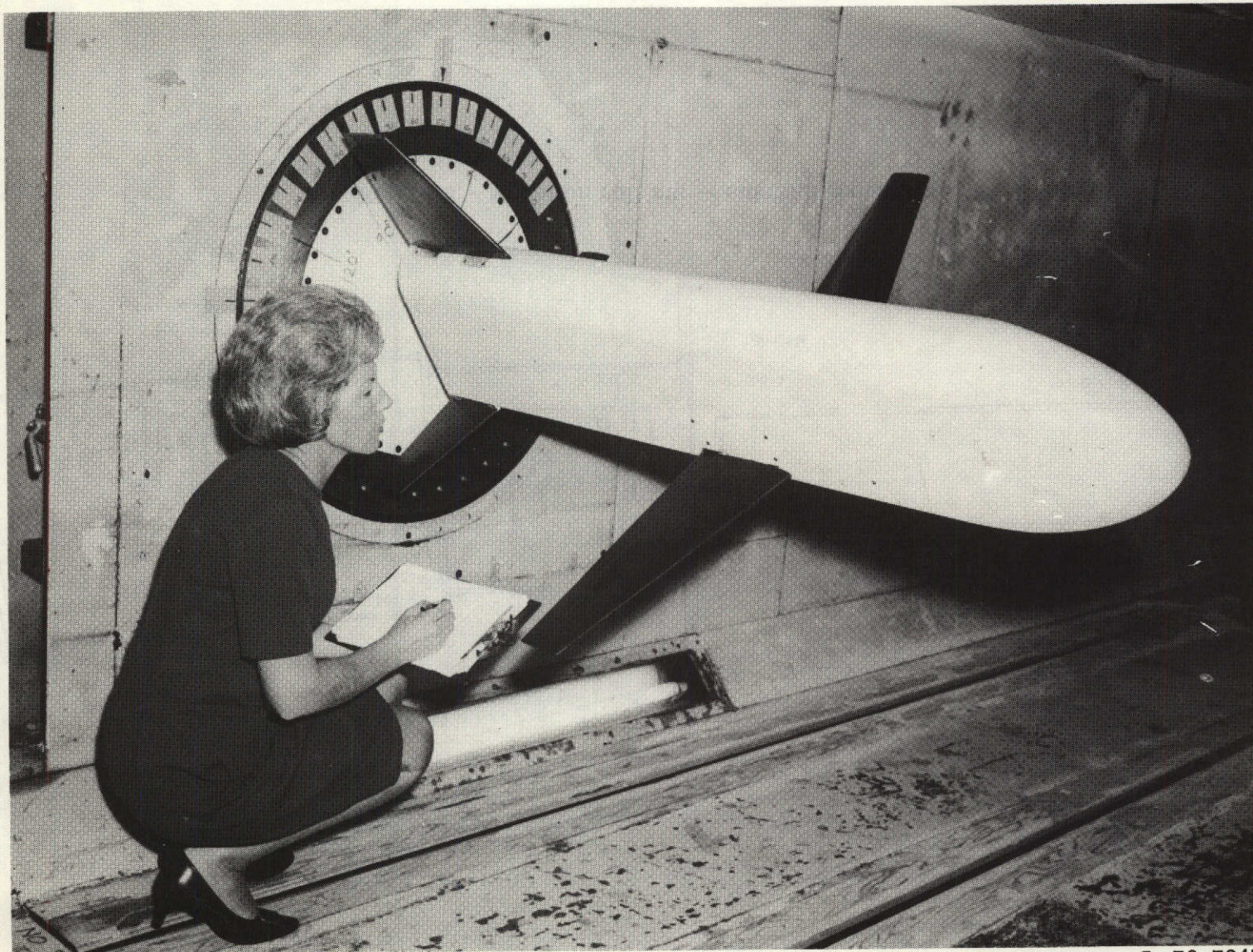
L-70-7347

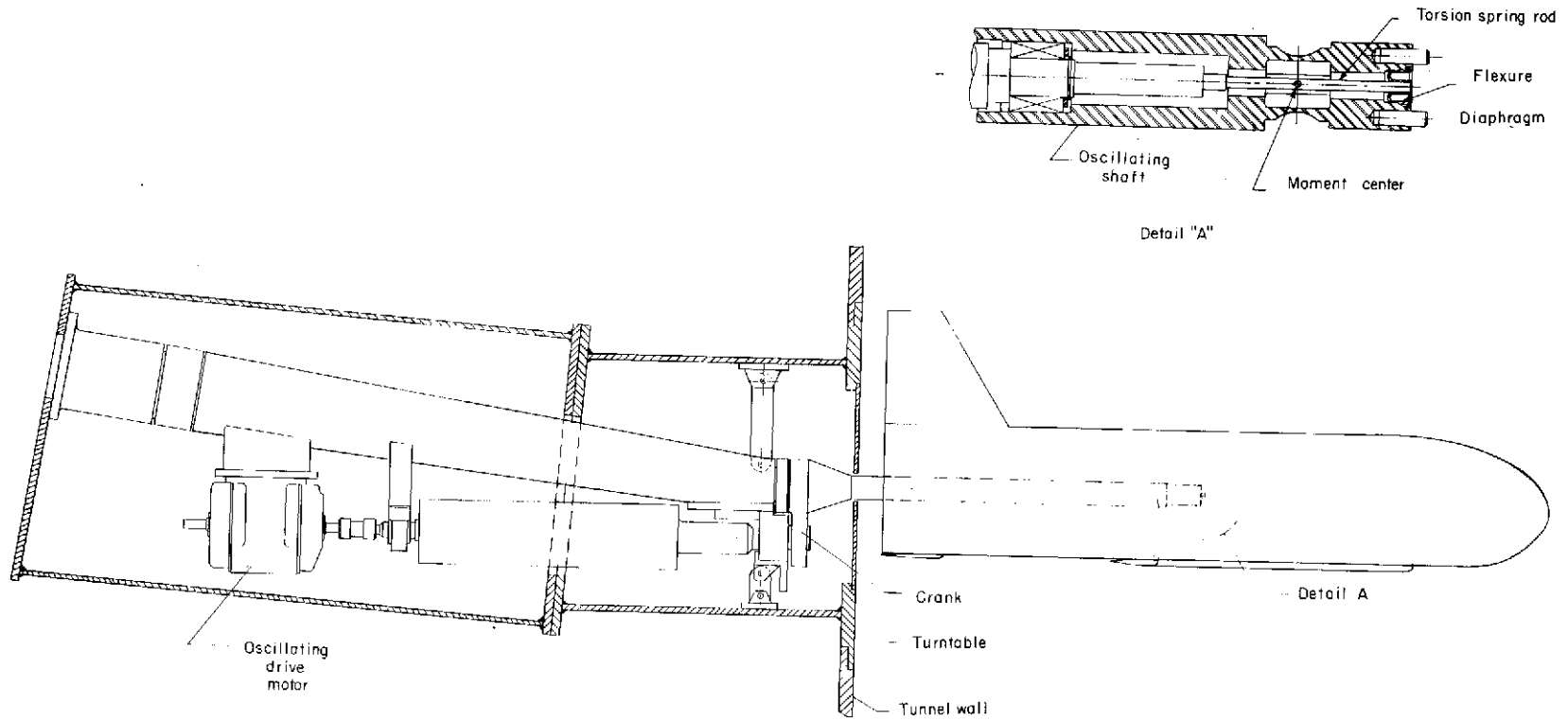Figure 2.- Model on oscillating sting balance.

Torsion spring rod

Flexure

Diaphragm

Oscillating
shaft

Moment center

Detail "A"

Oscillating
drive
motor

Crank

Turntable

Tunnel wall

Detail A

Figure 3.- Model on roll rig – sidewall mount.
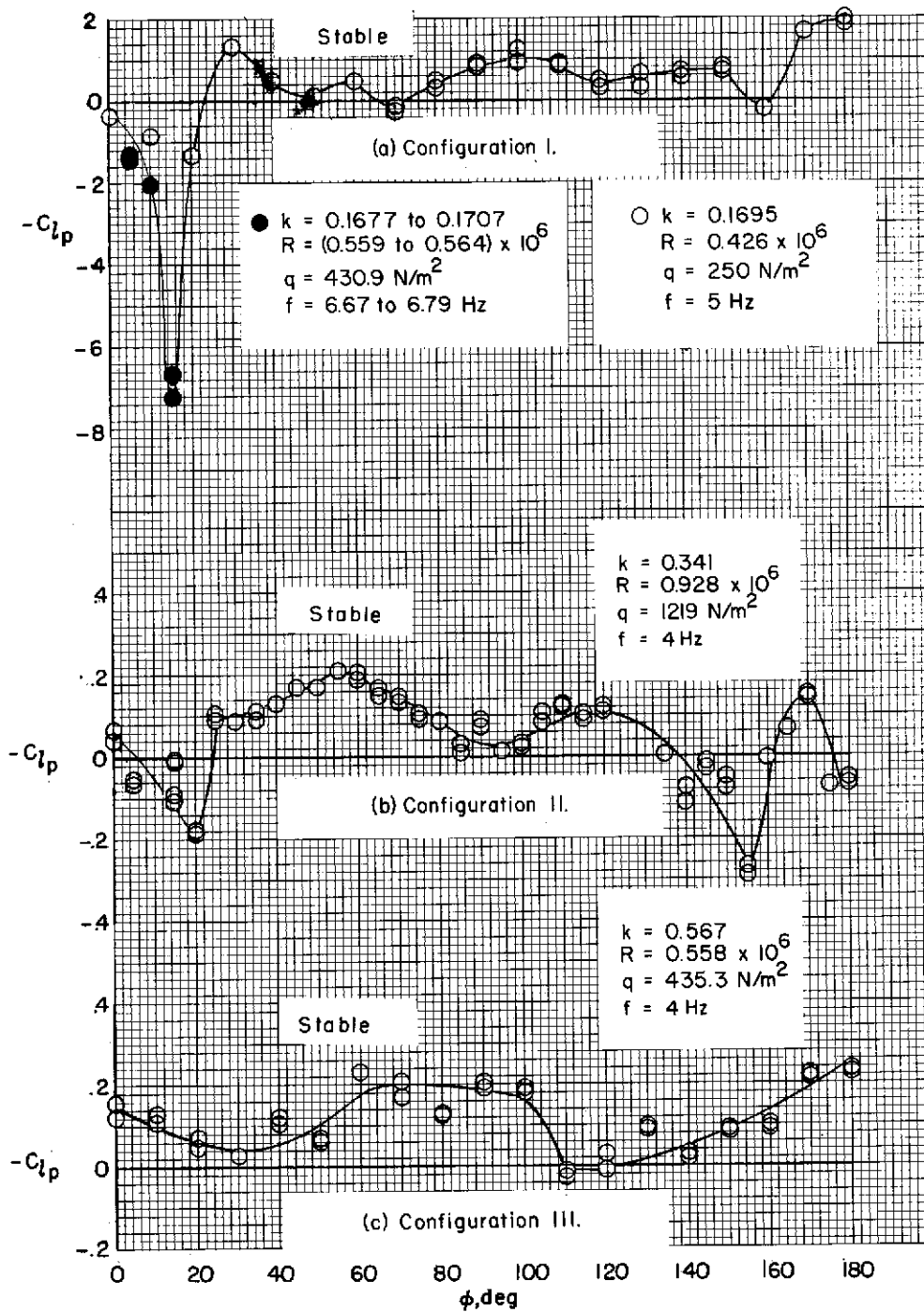
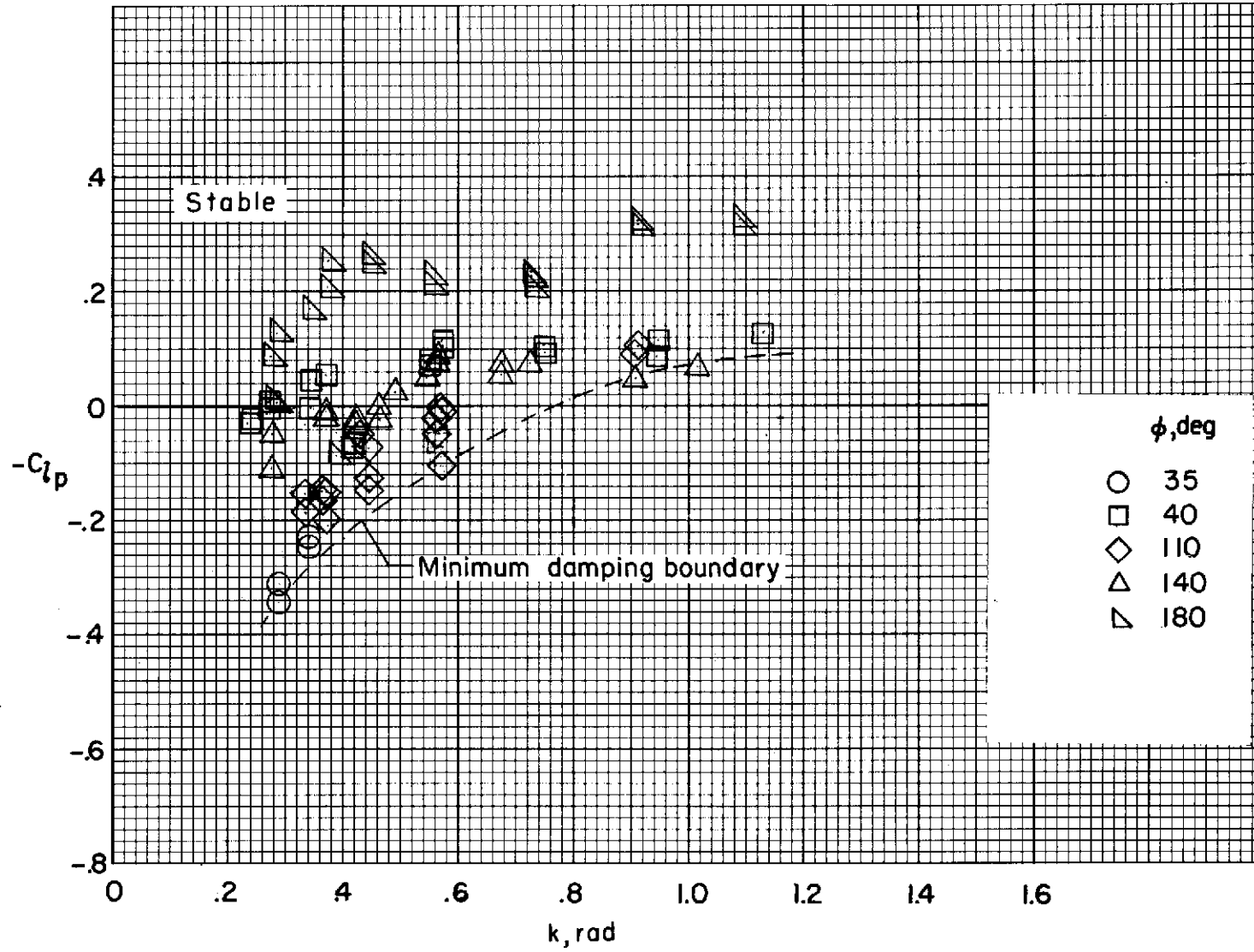Figure 4.- Aerodynamic damping in roll as a function of wind azimuth.
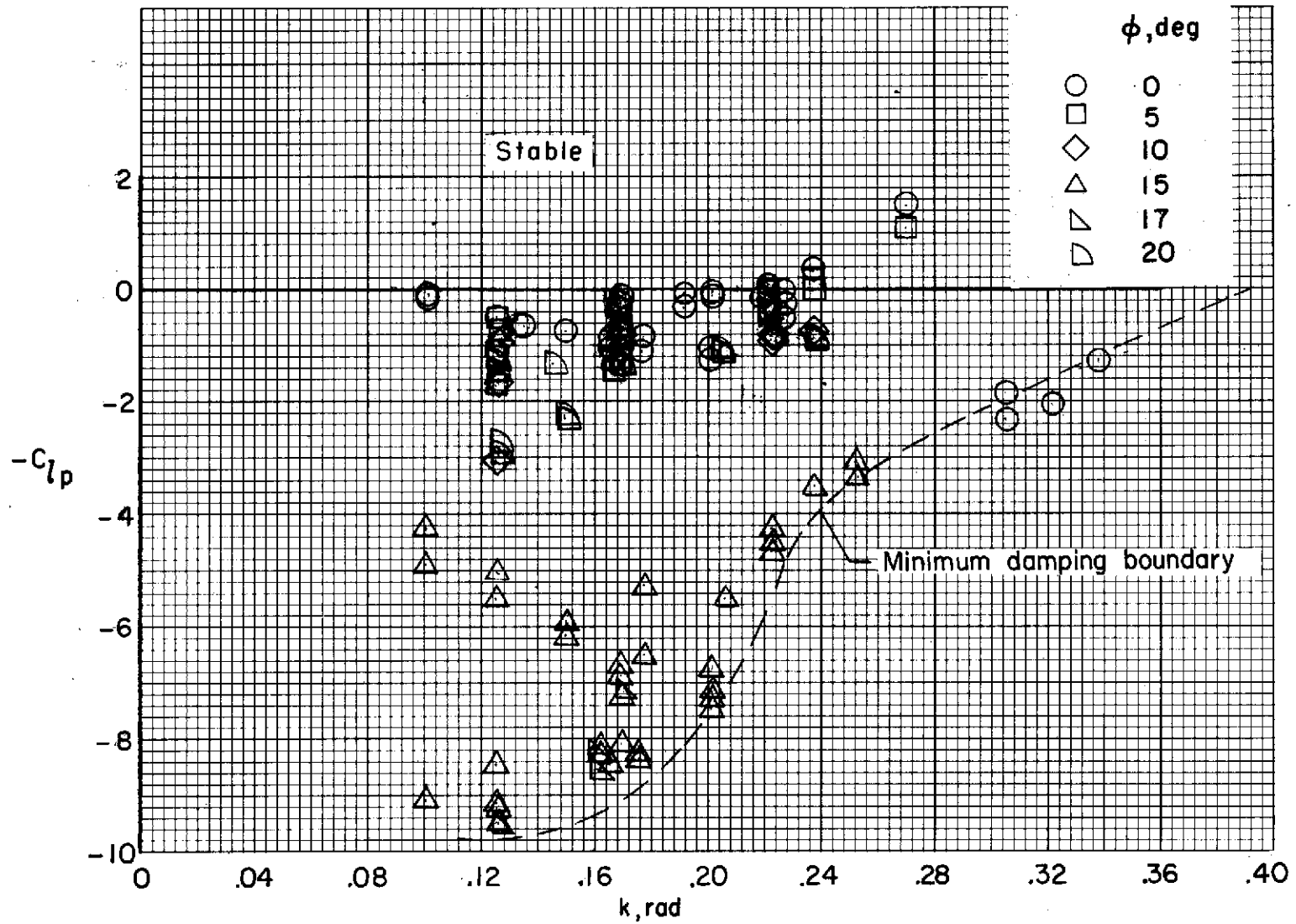
(a) Configuration I.

Figure 5.- Roll-damping characteristics as a function of reduced frequency.
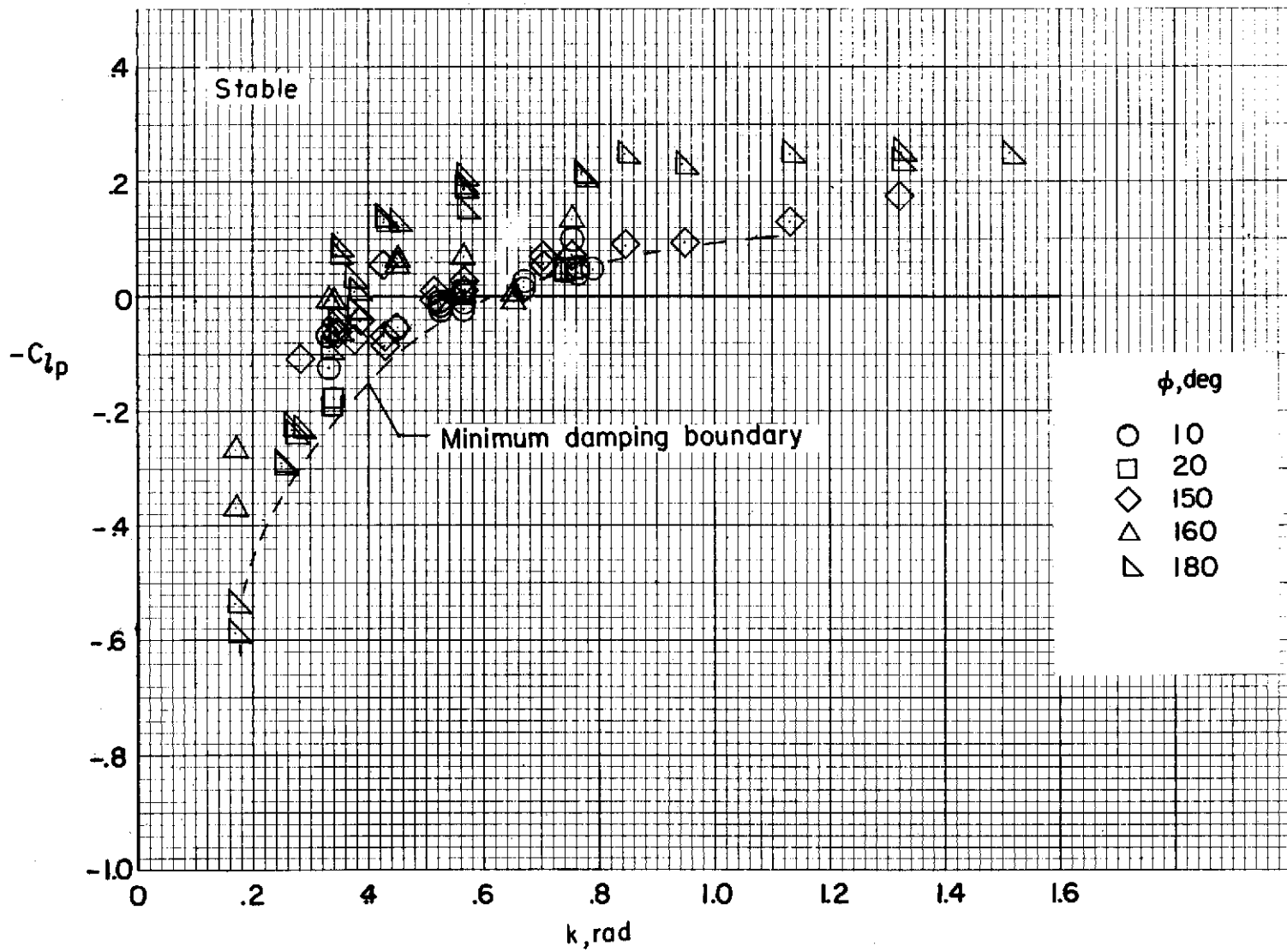
(b) Configuration II.

Figure 5.- Continued.
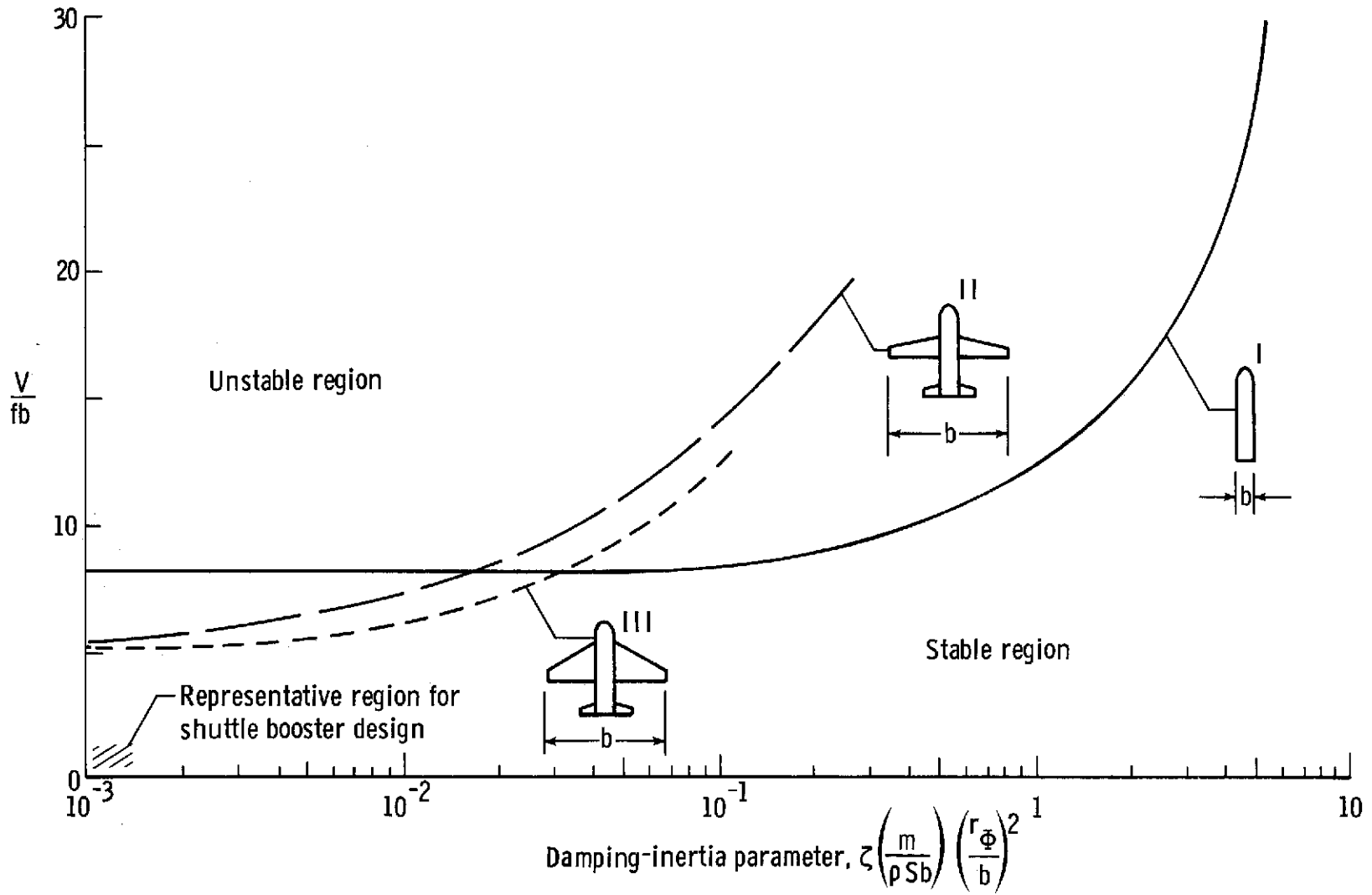
(c) Configuration III.

Figure 5.- Concluded.

Figure 6.- Stability boundaries as a function of reduced velocity and damping-inertia parameter.